Table S1. Statistics of model performance of different parameterization schemes for the hourly evolution of near-surface and vertical structure of specific humidity (Q), temperature (T), wind speed (WS), as well as atmospheric boundary layer height (ABLH) and precipitation (Preci) at Dezhou site (37.27°N, 116.72°E) during the winter sounding experiment (from December 26, 2017, to January 24, 2018).

		WSM6+GD			Lin+GD			WSM6+KF			Lin+KF		
		R	MB	RMSE	R	MB	RMSE	R	MB	RMSE	R	MB	RMSE
Q ($g\ kg^{-1}$)	surface	0.73	-0.19	0.59	0.69	-0.23	0.62	0.73	-0.19	0.6	0.71	-0.23	0.61
	vertical	0.61	0.04	0.43	0.58	0.03	0.43	0.59	0.03	0.43	0.58	-0.04	0.44
T (K)	surface	0.9	-1.45	2.7	0.89	-1.61	2.85	0.89	-1.44	2.73	0.88	-2.81	3.56
	vertical	0.97	-1.43	2.31	0.97	-1.39	2.3	0.97	-1.43	2.32	0.97	-1.98	2.55
WS ($m\ s^{-1}$)	surface	0.55	2.14	2.71	0.56	2.14	2.68	0.55	2.14	2.71	0.51	1.97	2.56
	vertical	0.52	0.72	3.44	0.52	0.70	3.43	0.51	0.74	3.46	0.51	0.69	3.47
ABLH (m)		0.71	-72	247	0.69	-81	259	0.71	-64	281	0.62	-137	299
Preci (mm/day)		0.99	0.01	0.05	0.68	0.05	0.16	0.89	0.01	0.06	0.78	0.03	0.12

Note. The temporal resolutions of sounding data and near-surface data are 3-hr and 1-hr, respectively, except for daily accumulated precipitation.

Table S2. Statistics of model performance of different parameterization schemes for the hourly evolution of near-surface and vertical structure of specific humidity (Q), temperature (T), wind speed (WS), as well as atmospheric boundary layer height (ABLH) and precipitation (Preci) at Dezhou site (37.27°N, 116.72°E) during the summer sounding experiment (from May 15 to June 14, 2018).

		WSM6+GD			Lin+GD			WSM6+KF			Lin+KF		
		R	MB	RMSE	R	MB	RMSE	R	MB	RMSE	R	MB	RMSE
Q ($g\ kg^{-1}$)	surface	0.81	-2.05	3.05	0.79	-2.16	3.22	0.81	-2.02	3.06	0.8	-2.13	3.16
	vertical	0.69	-0.29	2.18	0.67	-0.34	2.2	0.68	-0.32	2.18	0.67	-0.31	2.19
T (K)	surface	0.87	1.50	3.11	0.86	1.61	3.21	0.85	1.54	3.17	0.85	1.55	3.19
	vertical	0.95	1.89	2.83	0.91	1.94	3.23	0.93	2.21	3.15	0.91	2.29	3.56
WS ($m\ s^{-1}$)	surface	0.58	2.44	2.97	0.56	2.48	2.93	0.56	2.51	3.01	0.52	2.59	3.11
	vertical	0.54	1.10	3.21	0.53	1.16	3.34	0.52	1.10	3.4	0.5	1.21	3.57
ABLH (m)		0.84	121	343	0.79	146	379	0.82	132	379	0.8	139	387
Preci (mm/day)		0.91	-0.59	2.79	0.83	-0.93	3.77	0.87	-0.76	3.11	0.85	-0.88	3.35

Note. The temporal resolutions of sounding data and near-surface data are 3-hr and 1-hr, respectively, except for daily accumulated precipitation.

Table S3. Statistics of mean, standard deviation, and Kolmogorov-Smirnov test significance for the key meteorological elements at near-surface and 700 hPa over 30 years of historical data (1990-2019) and 7 years of the sampling period (2011&2014-2019).

Variables		30-year mean±adv	7-year mean±adv	K-S Sig. ($p<0.05$)
ABLH (m)		469.7±91.9	470.3±90.1	1.000
Preci (mm)		3.55±2.01	3.36±1.83	0.938
Near surface	U ($m\ s^{-1}$)	-0.29±0.28	-0.30±0.28	0.890
	V ($m\ s^{-1}$)	-0.07±0.66	-0.10±0.65	0.999
	T (K)	287.8±8.2	288.0±8.2	0.983
700hPa	U ($m\ s^{-1}$)	4.84±2.05	4.72±2.01	0.991
	V ($m\ s^{-1}$)	0.60±1.28	0.59±1.13	0.882
	W ($Pa\ s^{-1}$)	-0.006±0.019	-0.005±0.017	0.993
	Q ($g\ kg^{-1}$)	4.79±2.06	4.87±2.14	0.986
	T (K)	276.6±5.6	276.8±5.7	0.995

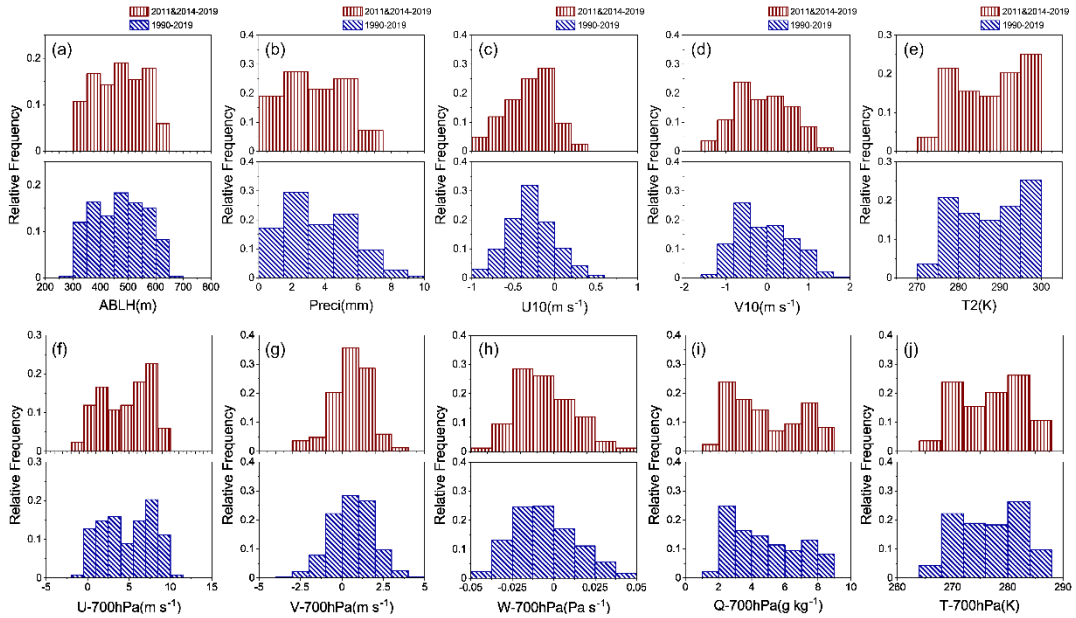

Figure S1. Histogram of the (a) boundary layer height, (b) precipitation, (c-d) 10 m horizontal winds, (e) 2 m temperature, as well as (f-h) three-dimension wind component, (i) specific humidity, (j) temperature at 700 hPa during 7-year sample (2011&2014-2019, filled with brown vertical lines) and 30-year climatology (1990-2019, filled with blue oblique lines).

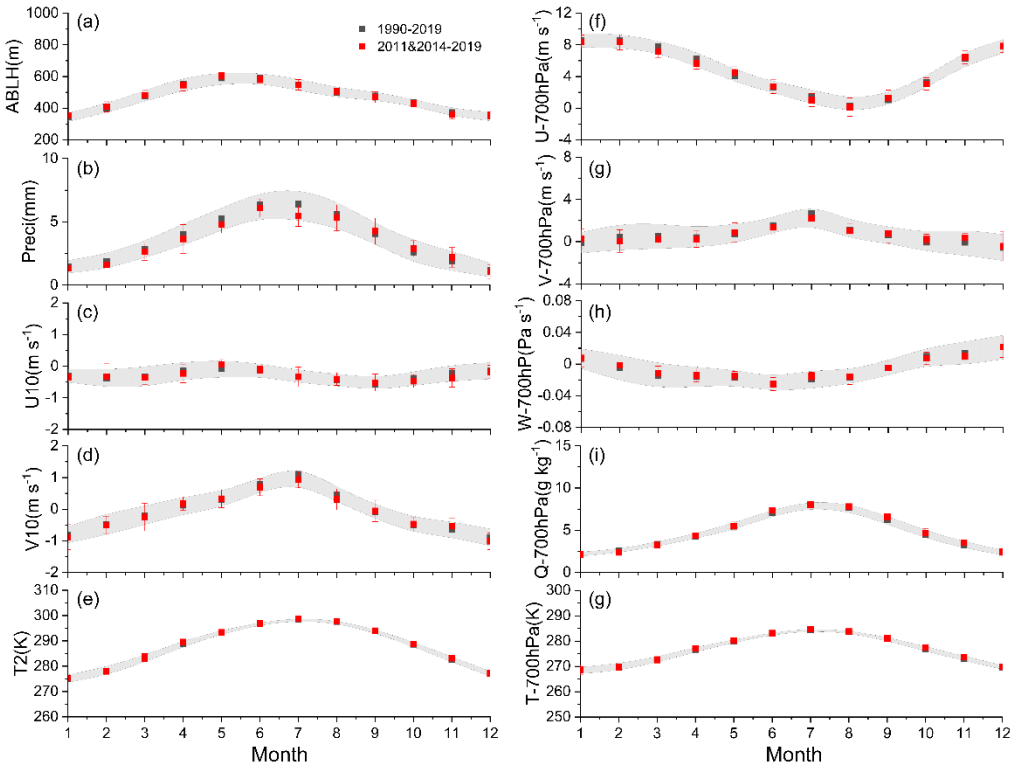

Figure S2. Annual variation of the monthly average with standard deviation for (a) boundary layer height, (b) precipitation, (c-d) 10 m horizontal winds, (e) 2 m temperature, as well as (f-h) three-dimension wind component, (i) specific humidity, (j) temperature at 700 hPa during 7-year sample (2011&2014-2019, red square with line) and 30-year climatology (1990-2019, black square with gray-shaded area).

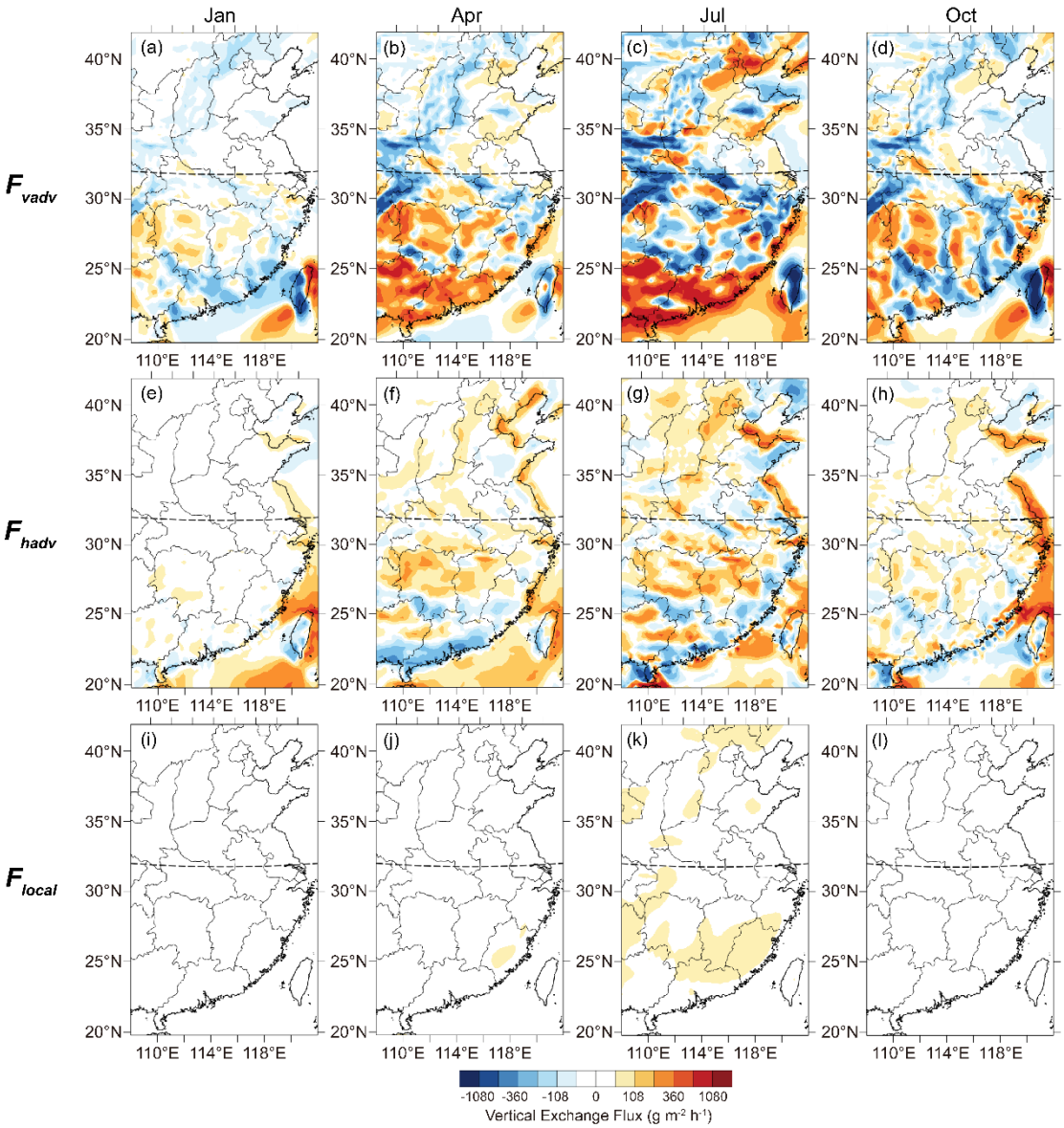

Figure S3. Spatial distribution of three average flux components of ABL-FT water vapor exchange (F_{vadv}, a-d; F_{hadv}, e-h; F_{local}, i-l) averaged over 7-year for January, April, July, and October. Positive and negative fluxes (warm and cool colors) represent water vapor upward and downward transport at the ABL and FT interface. Black dashed lines mark the boundary between the northern (32-42°N, 108-122°E) and southern (20-32°N, 108-122°E) regions.

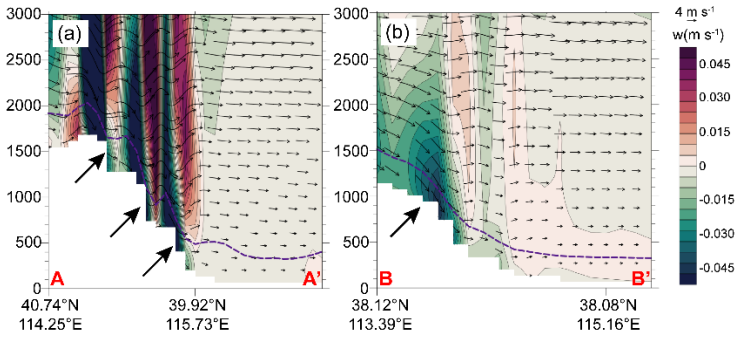

Figure S4. The height cross-sections of vertical velocity superimposed with u-w wind vectors (w multiplied by 100) averaged over 7-year for January. Cross sections extracted from (AA': 41.21°N, 115.15°E) to (39.09°N, 117.20°E) and from (BB': 38.1°N, 113.45°E) to (38.1°N, 115.47°E), respectively. The thin arrows, purple dashed lines and bold arrows indicate u-w wind vectors, ABL heights and steep/gentle slopes, respectively.

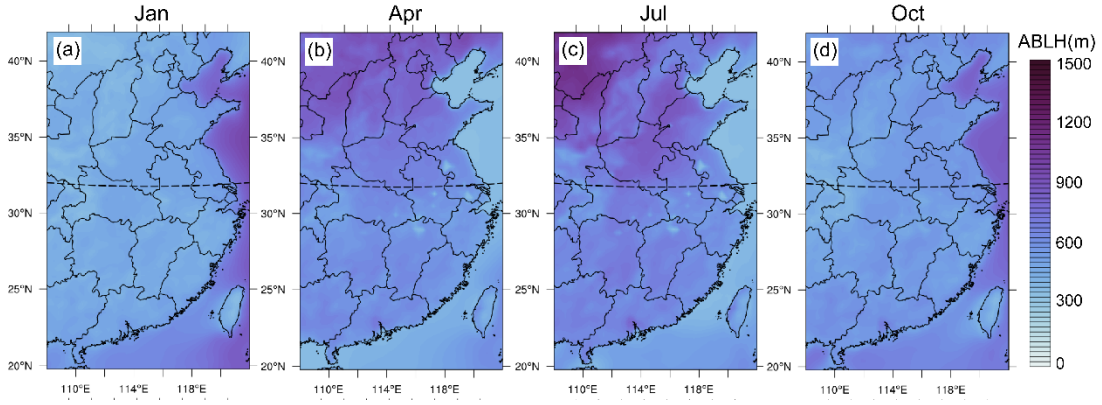

Figure S5. Spatial distribution of ABL height averaged over 7-year for (a) January, (b) April, (c) July, and (d) October. Black dashed lines mark the boundary between the northern (32-42°N, 108-122°E) and southern (20-32°N, 108-122°E) regions.

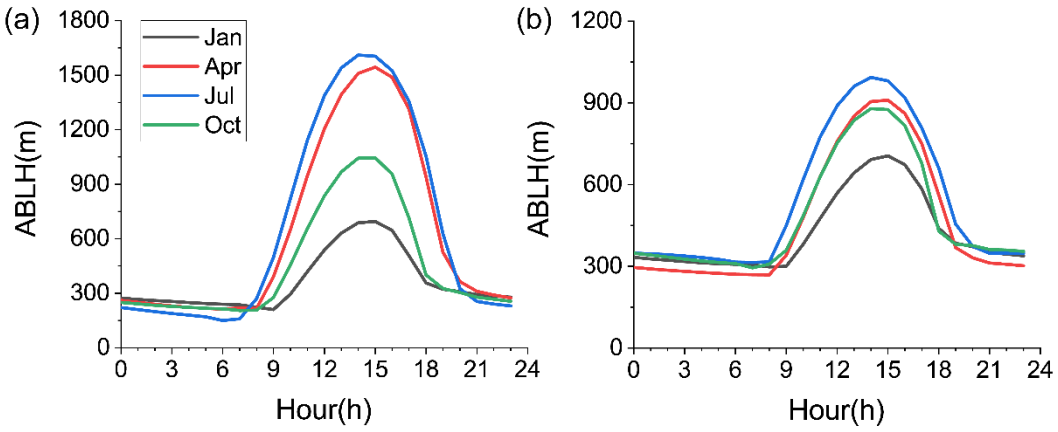

Figure S6. Daily cycle of ABL height over the (a) northern (32-42°N, 108-122°E) and (b) southern (20-32°N, 108-122°E) regions averaged over 7-year for January, April, July, and October.